

An Epilepsy-Related ARX Polyalanine Expansion Modifies Glutamatergic Neurons Excitability and Morphology Without Affecting GABAergic Neurons Development

Shirley Beguin^{1,2,3}, Valérie Crépel^{1,2,3}, Laurent Aniksztejn^{1,2,3}, H  l  ne Becq^{1,2,3}, Barbara Pelosi⁴, Emilie Pallesi-Pocachard^{1,2,3}, Lamine Bouamrane^{1,2,3}, Massimo Pasqualetti⁴, Kunio Kitamura⁵, Carlos Cardoso^{1,2,3} and Alfonso Represa^{1,2,3}

¹INSERM Unit   901, Marseille 13009, France ²Aix-Marseille Universit  , UMR S901, Universit   de la M  diterran  e, Marseille 13009, France ³INMED, Marseille 13009, France ⁴Department of Biology, University of Pisa, 56127 Pisa, Italy ⁵Department of Mental Retardation and Birth Defect Research, National Institute of Neuroscience, National Center of Neurology and Psychiatry, Tokyo 187-8502, Japan

Address correspondence to Alfonso Represa, INMED/INSERM Unit   901, 163 Route de Luminy BP 13, 13273 Marseille cedex 09, France. Email: represa@inmed.univ-mrs.fr.

Epileptic encephalopathies comprise a heterogeneous group of severe infantile disorders for which the pathophysiological basis of epilepsy is inaccurately clarified by genotype–phenotype analysis. Because a deficit of GABA neurons has been found in some of these syndromes, notably in patients with X-linked lissencephaly with abnormal genitalia, epilepsy was suggested to result from an imbalance in GABAergic inhibition, and the notion of “interneuronopathy” was proposed. Here, we studied the impact of a polyalanine expansion of aristaless-related homeobox (ARX) gene, a mutation notably found in West and Ohtahara syndromes. Analysis of *Arx*^{(GCG)⁷/Y} knock-in mice revealed that GABA neuron development is not affected. Moreover, pyramidal cell migration and cortical layering are unaltered in these mice. Interestingly, electrophysiological recordings show that hippocampal pyramidal neurons displayed a frequency of inhibitory postsynaptic currents similar to wild-type (WT) mice. However, these neurons show a dramatic increase in the frequency of excitatory inputs associated with a remodeling of their axonal arborization, suggesting that epilepsy in *Arx*^{(GCG)⁷/Y} mice would result from a glutamate network remodeling. We therefore propose that secondary alterations are instrumental for the development of disease-specific phenotypes and should be considered to explain the phenotypic diversity associated with epileptogenic mutations.

Keywords: ARX, epilepsy, network excitability, neuronal migration

Introduction

Epileptic encephalopathies comprise a large group of conditions in which cognitive function deteriorates as a consequence of epileptic activity (Korff and Nordli 2006; Nabbout and Dulac 2008). Although different genes have been identified (reviewed in Nabbout and Dulac 2008), the origin of the epileptic condition remains unclear in many cases. Furthermore, the high diversity of syndromes linked to a same gene and the observation that alterations of different genes yield the same phenotype make any clinical investigation problematic.

ARX (aristaless-related homeobox) gene is implicated in a wide spectrum of X-linked neurological disorders, which extend from less severe phenotypes characterized by mental retardation with no apparent brain developmental abnormalities to extremely severe phenotypes such as X-linked lissencephaly associated with abnormal genitalia (XLAG) (reviewed in Kato et al. 2004; Friocourt et al. 2006; Gecz et al. 2006; Shoubridge et al. 2010). Thus far, genotype–phenotype analysis has failed to clarify the biological/ pathophysiological basis for this pleiotropy.

It has been proposed that epileptogenesis in these patients could result primarily from a deficit of GABA inhibition (Kato and Dobyns 2005). Thus, *Arx* protein is highly expressed in GABA interneurons (Kitamura et al. 2002; Colombo et al. 2004; Poirier et al. 2004) and has been found to be important for their tangential migration from the ganglionic eminences to the cortical fields (Kitamura et al. 2002; Colombo et al. 2007; Friocourt et al. 2008). Furthermore, a decrease in GABA neurons has been reported in cortical samples from lissencephalic patients with *ARX* mutations (Bienvenu et al. 2002; Okazaki et al. 2008; Marcorelles et al. 2010). However, it is known that the majority of *ARX* mutations are not associated with brain malformations (Shoubridge et al. 2010). This is the case for the insertion of 7 tandem GCG repeats within the normal stretch of the first polyalanine tract (amino acids 100–115), a mutation reported to cause severe epilepsy syndromes: X-linked West syndrome (Stromme et al. 2002), infantile spasms and status dystonicus (Guerrini et al. 2007), and Ohtahara syndrome (Absoud et al. 2010). It is presently unclear whether this mutation also affects migration and differentiation of GABA interneurons. Two groups have reproduced this mutation in mice (Kitamura et al. 2009; Price et al. 2009). When compared with X-linked lissencephaly mice (Kitamura et al. 2002, 2009), these mice display more moderate brain alterations but exhibit a severe epilepsy, making it possible to evaluate, in relevant animal models, the contribution of an imbalance of GABA in epileptic manifestations.

In this report, we analyzed *Arx*^{(GCG)⁷/Y} mice (Kitamura et al. 2009) in order to evaluate at both structural and electrophysiological levels how this mutation could impact GABAergic inhibition. We demonstrate here that the distribution and density of GABA neurons, which migrate to the cortical and hippocampal fields, remain unaffected by the mutation and, consistent with this, the frequency of spontaneous GABA-mediated inhibitory postsynaptic currents (IPSCs) in hippocampal neurons from *Arx*^{(GCG)⁷/Y} mice does not differ from that of WT animals. Surprisingly, our data further suggest that epilepsy in *Arx*^{(GCG)⁷/Y} mice results from glutamatergic network reorganization, as illustrated by a dramatic increase in the frequency of spontaneous excitatory glutamate-mediated postsynaptic currents (EPSCs) in CA1 pyramidal neurons together with an abnormal distribution of their axon collaterals. Because glutamatergic neurons do not express *Arx*, the morphofunctional changes described here most likely result from noncell autonomous effects. This indicates that brain changes secondary to the original mutation strongly contribute to the development of disease-specific phenotypes.

Materials and Methods

Animals

For our study, Wistar rats (Janvier, France) were used. Mouse experiments were performed on *Arx*^{(GCG)7} (330 position) knock-in mice (developed and kindly provided by Dr Kunio Kitamura, Mitsubishi Kagaku Institute of Life Sciences) available in the RIKEN BioResource Center in Japan [strain name: *Arx*(GCG)7-1 KI (B6), RBRC03654]. Mice were maintained by crossing heterozygous females (*Arx*^{(GCG)7/X}) with WT males C57BL/6J. Genotyping was performed according to the protocol of the RIKEN BioResource Center. All animal handling and care procedures were in accordance with the European Union and French legislation.

Plasmid Constructs and Western-Blot Analysis

For control experiments, pCAGIG vectors (Addgene) or pCAGGS-red fluorescent protein (RFP, a gift from Dr LoTurco) was used. RNA interference experiments were performed with 2 shRNAs targeting either the coding sequence [Sh2; nucleotides 708–730 (homologous to S2 described by Friocourt et al. 2008)] or the 3' UTR (shC; nucleotides 1954–1977) of *Rattus norvegicus Arx* mRNA (GenBank accession number: EF638804). As negative controls, we used 2 corresponding nontargeting mismatch shRNAs ms2 and msC. These shRNAs were subcloned into an mU6pro vector (a gift from Dr LoTurco). The human ARX(GCG)7 cDNA (Shoubbridge et al. 2007) was inserted into the EcoRI–EcoRV sites of the pCAGIG vector, generating the pCAGIG-ARX(GCG)7 plasmid. To generate the WT human ARX cDNA, the primers CTAAGAGCAGCAGCGCCCGT and CGTCTCCAGCAGTTCCTCTTC were used to PCR amplify from WT human genomic DNA a 536 bp fragment containing the region of the first polyaniline stretch.

To obtain the pCAGIG-ARX WT human expression vector, the amplified fragment was digested with NaeI–EcoNI and then subcloned in NaeI–EcoNI of the pCAGIG-ARX(GCG)7 plasmid to replace the fragment containing the (GCG)7 expansion.

The newly generated plasmids were fully sequenced to exclude the presence of mutations.

Plasmids used for in utero electroporation were prepared using the EndoFree Plasmid kit (Qiagen).

Efficacies of our constructs were tested on HEK 293 cells 48 h after transfection with the CombiMag reagent (OZ-Biosciences, France), according to the manufacturer's protocol and subsequent western blot analysis (Supplementary Fig. S1). Cells were lysed in a buffer (150 mM NaCl, 50 mM Tris–HCl pH 8.0, 50 mM NaF, 0.5% Nonidet P40, 2 mM EDTA, protease inhibitor cocktail) at 4°C before proteins were heat denatured and processed by sodium dodecyl sulfate–polyacrylamide gel electrophoresis, transferred to nitrocellulose, and immunoblotted with the following primary antibodies: *Arx* (a gift from Dr Collombat, 1/1000), alpha-tubulin (Sigma, St Louis, MO, USA, 1/10 000), and green fluorescent protein (GFP) (Chemokine, 1/5000). The proteins were detected with the Western Lumi-Light kit chemiluminescence reagent (Roche).

In Utero Electroporation

Timed pregnant mice (E14) were anesthetized with ketamine/xylazine (100 and 10 mg/kg, respectively). The uterine horns were exposed. An aliquot of 1–2 μ L of DNA plasmid (pCAGGS-RFP) either alone (1.5 μ g/ μ L) or combined (0.5 μ g/ μ L) with 1.5 μ g/ μ L of Sh2 shRNA construct or ARX(GCG)7 human combined with Fast Green (2 mg/mL, Sigma) was injected into the lateral ventricle of each embryo with a pulled glass capillary and a microinjector (Picospritzer II, General Valve Corporation, Fairfield, NJ, USA). Electroporation was then conducted by discharging a 4000 μ F capacitor charged to 50 V with a BTX ECM 830 electroporator (BTX Harvard Apparatus, Holliston, MA, USA). Five electric pulses (5 ms duration) were delivered at 950 ms intervals with electrodes placed to target cortical ventricular progenitors. Embryos were then allowed to develop for 4 days, and the positions of transfected cells were analyzed on a laser-scanning confocal microscope (FluoView 300, Olympus). Cortical quantification was performed with eCELLence software (www.gvt.it/ecellence) on

coronal sections (100 μ m) located in the dorsolateral neocortex. Relative positions of transfected cells were estimated by counting RFP-positive cells in 10 areas from deep to superficial layers and calculated in percentage, compared with the total number of electroporated cells.

Analyses of interneuron migration were conducted on coronal sections (100 μ m) with the ImageJ software 1.44j. The number of electroporated cells in the cortex and in the ganglionic eminence was counted, and the percentage of electroporated cells in the cortex versus the ganglionic eminence was calculated for each section.

Immunohistochemistry and Antibodies

Mouse brains were rapidly removed and fixed (embryonic brains) or perfused (postnatal brains) with Antigenfix solution (Diapath). Brains were then embedded in 4% agar and sectioned at 100 μ m with a Vibratome (Microm). Sections were blocked with 5% normal goat serum in phosphate-buffered saline (PBS) and 0.3% Triton X-100 for 1 h and incubated with the appropriate primary antibody overnight at 4°C, for interneuron quantification: ARX (a gift from Dr Chelly, 1/1000), GABA (Sigma, A2052, 1/16 000), Calbindin (Chemicon, AB1778, 1/1000), Calretinin (Chemicon, AB5054, 1/1000), and Parvalbumin (Sigma, AB15738, 1/1000); for neurons staining: NeuN (Millipore, MAB377, 1/500); and for cortical layer analysis: CDP (M-222, sc-13024 Santa Cruz, 1/100), FoxP2 (Abcam Ab16046, 1/500), and Bc11b (Novus biological, NB100-2600, 1/250). After 3 washes in PBS, sections were incubated with Alexa Fluor 488- or 647- or 555-conjugated secondary antibody (Invitrogen) in a 1:500 dilution at room temperature for 2 h, washed, and mounted with Fluoromount G mounting medium (SouthernBiotech). Images were acquired with a laser-scanning confocal microscope (FluoView 300, Olympus) or with an Apotome (Zeiss).

Interneuron quantification was performed with the ImageJ software 1.44j. Positive cells were counted in a pixel square containing all cortical layers, and then we reported these numbers in percentage of positive cells per millimeter compared with the control condition considered as 100%. Cortical layer analyses were made with the ImageJ software 1.44j. The cortical thickness of each cortical layer was measured in millimeters for each analyzed section.

Primary Hippocampal Cultures, Transfections, and Immunocytochemistry

Hippocampal neurons from 18-day-old rat embryos were dissociated using trypsin and plated at a concentration of 200 000 cells/mL in minimal essential medium supplemented with 10% Nu-Serum (Becton Dickinson), 0.45% glucose, 1 mM sodium pyruvate, 150 mM HEPES, and 10 IU/mL penicillin–streptomycin. Transfections of 3 days *in vitro* (DIV) neuronal cultures were performed with the CombiMag reagent (OZ-Biosciences), according to the manufacturer's protocol. Transfection was terminated by substituting 90% of the incubation solution with fresh culture media. Cells were fixed in Antigen solution (Diapath) 3 days after transfection. After 3 washes in PBS, cells were blocked with 5% normal goat serum in PBS and 0.3% Triton X-100 for 1 h and incubated with the GAD67 primary antibody (Millipore MAB5406, 1/500) overnight at 4°C. After 3 washes in PBS, cells were incubated with Alexa Fluor 555-conjugated secondary antibody (Invitrogen) in a 1:500 dilution at room temperature for 2 h, washed, and mounted with Fluoromount G mounting medium (SouthernBiotech). Cells positive for GAD67 staining were analyzed on a laser-scanning confocal microscope (FluoView 300, Olympus). Morphological analyses were performed on the ImageJ software 1.44j with the NeuronJ plugin.

Electrophysiological Recordings

Knock-in mice *Arx*^{(GCG)7/Y} at P15–P17 were used for these experiments. At these stages, no generalized seizures were visually observed. Animals were decapitated under deep isoflurane anesthesia (20–40 mg/kg). The brain was removed rapidly, the hippocampi and the neocortex were dissected, and transverse 400 μ m thick slices were cut using an HM650V MicroM tissue slicer in a solution containing the

following (in mM): 110 choline, 2.5 KCl, 1.25 NaH₂PO₄, 25 NaHCO₃, 7 MgCl₂, 0.5 CaCl₂, and 7 D-glucose (5°C). Slices were then transferred for rest at room temperature (1 h) in oxygenated normal artificial cerebrospinal fluid (ACSF) containing the following (in mM): 126 NaCl, 3.5 KCl, 1.2 NaH₂PO₄, 26 NaHCO₃, 1.3 MgCl₂, 2.0 CaCl₂, and 10 D-glucose, pH 7.4.

Individual slices were then transferred to the recording chamber, where they were fully submerged and superfused with ACSF at 32°C at a rate of 2–3 mL/min. CA1 pyramidal cells were recorded in whole-cell configuration in current-clamp mode with microelectrodes filled with a solution containing (in mM): 130 KM₂SO₄, 10 KCl, 0.1 CaCl₂, 1.1 EGTA, 10 HEPES, 4 Mg²⁺ ATP, and 0.3 Na⁺ GTP, pH 7.25, 270–280 mOsm, or in voltage-clamp mode with microelectrodes containing (in mM): 130 CsGlu, 10 CsCl, 0.1 CaCl₂, 1.1 EGTA, 10 HEPES, 4 Mg²⁺ ATP, and 0.3 Na⁺ GTP. Biocytin (0.5%) was added to the pipette solution for post hoc reconstruction.

Whole-cell measurements were made in voltage-clamp or current-clamp mode using a Multiclamp 700 A amplifier (Axon Instruments, Molecular Devices, Union City, CA, USA). Data were filtered at 2–3 kHz, digitized (20 kHz) with a Digidata 1200 and 1322A (Molecular Devices) to a personal computer, and acquired using Axoscope 7.0 and Clampex 9.2 software (PCLamp, Axon Instruments, Molecular Devices). Signals were analyzed off-line using MiniAnalysis 6.0.1 (Synaptosoft, Decatur, GA, USA) and Clampfit 10.1 (Molecular Devices).

Extracellular recordings were performed with a glass pipette filled with ACSF and positioned in CA1 stratum pyramidale; the signal was recorded with a DAM80 amplifier (WPI).

All values are given as mean ± SEM. The level of significance was set at $P < 0.05$, and n refers to the number of cells, except when otherwise stated.

Biocytin Staining and Analysis

Hippocampal and neocortical slices were fixed with Antigenfix (Diapath) overnight at 4°C. After 3 washes in PBS, slices were incubated in PBS 20% sucrose overnight at 4°C. Slices were then frozen in liquid nitrogen for cryoprotection and washed 3 times in PBS. Sections were blocked with 5% normal goat serum in PBS and 0.5% Triton X-100 for 1 h at room temperature. Slices were incubated with Streptavidin-Cy3 (GE Healthcare, 1/1000) in PBS 0.3% Triton and normal goat serum (1/200), overnight at room temperature. After 3 washes in PBS, sections were mounted with Fluoromount G mounting medium (SouthernBiotech). Biocytin-positive cells were imaged with a laser-scanning confocal microscope (FluoView 300, Olympus) and analyzed with the NeuroLucida software (mbf Bioscience).

Statistical Analysis

Statistical analysis was performed with SigmaStat 3.1 (Systat Software). A 2-sample Student's t -test was used to compare means of 2 independent groups if distribution of data was normal. When the normality test failed, the nonparametric Mann–Whitney test was used.

Results

The Distribution and Density of Cortical and Hippocampal Interneurons are Unaffected by ARX(GCG)7 Mutation

Arx is highly expressed in interneurons (Kitamura et al. 2002; Colombo et al. 2004; Poirier et al. 2004) and is required for their correct migration (Kitamura et al. 2002; Colombo et al. 2007; Friocourt et al. 2008). A recent report by Nasrallah et al. (2011) reported that ARX(GCG)7 mutation in organotypic slices affected the migration of neurons from the medial ganglionic eminence. However, previous studies suggest that ARX(GCG)7 mutation results in a relatively moderate loss of GABA interneurons in knock-in mice (Kitamura et al. 2009;

Price et al. 2009). To determine whether this polyalanine expansion results in a loss of GABAergic neurons in the cortex and hippocampus, we evaluated the number of interneurons in mice with the ARX(GCG)7 mutation. We stained P14–P15 cortical and hippocampal sections with interneuronal markers GABA, ARX, Calbindin, Calretinin, and Parvalbumin, and we found no alterations in the distribution or in the number of cells immunopositive for these markers in the neocortices and hippocampi of Arx(GCG)7/Y when compared with Arx^{X/Y} mice (Fig. 1*a–g* and Supplementary Fig. S2).

The Morphology of Interneurons is Unaffected by ARX(GCG)7 Mutation

Previous studies have suggested that alterations in the Arx gene could disrupt the morphology of interneurons (Colombo et al. 2007; Friocourt et al. 2008). We thus examined whether the ARX(GCG)7 mutation could result in an altered maturation of interneurons in primary cultures of rat hippocampal neurons. Transfections with plasmid constructs were performed at 3 DIV, and GAD67 immunostaining was performed 72 h later in order to specifically analyze the morphology of transfected interneurons (Fig. 2*a–c*). When compared with control interneurons expressing a mismatch construct ($n = 33$ cells) (Fig. 2*a*), we found that RNAi-mediated Arx knockdown in cultivated interneurons ($n = 36$ cells) resulted in a wider neuritic outgrowth (Fig. 2*b*), as illustrated by the increased number of dendritic branch points ($60.8 \pm 13.49\%$ and $73 \pm 14.78\%$ for Sh2 and shC, respectively; Mann–Whitney test $P = 0.01$ and 0.001 , respectively; Fig. 2*d,e*); the number of primary dendrites, however, was not modified. Associated with this increased branching, the total dendritic length was also significantly increased by $31.78 \pm 9.47\%$ (Sh2; Mann–Whitney test $P = 0.009$) and $49.82 \pm 14.07\%$ (shC; Mann–Whitney test $P = 0.005$). Interneurons transfected with ARX(GCG)7 human mutation (Fig. 2*c*), whether combined with shRNA or mismatch constructs, presented a normal dendritic tree in terms of dendritic length, number of primary dendrites (ca. 2.7; Fig. 2*d*), and number of branching points (Fig. 2*e*) when compared with cells transfected with GFP or ARX WT human form or mismatch constructs (Fig. 2*d,e*). These data show that Arx is required for interneuronal maturation when it exerts a “repressor” action on dendritic branching and outgrowth. Our data also suggest that (GCG)7 polyalanine expansion does not alter this effect in vitro. The analysis of presumptive pyramidal cells (cells immunonegative for GAD67 antibodies are also ARX-negative) indicates that transfection with ARX WT or ARX(GCG)7 constructs did not affect neurite outgrowth, whereas their transfection with ARX shRNA vectors failed to induce any significant change, as expected.

To further examine the impact of ARX(GCG)7 mutation on neuritic outgrowth, we reconstructed the dendritic arbor of stratum oriens interneurons injected with biocytin in acute hippocampal sections from transgenic mice (Fig. 2*f–i*). We did not observe any significant change between Arx^{X/Y} ($n = 6$) and Arx^{(GCG)7/Y} ($n = 6$) mice neither in the total dendritic length (Fig. 2*b*) nor in the number of branch points (Fig. 2*i*). Overall, these results show that the ARX(GCG)7 mutation has no major effect on interneuron morphology.

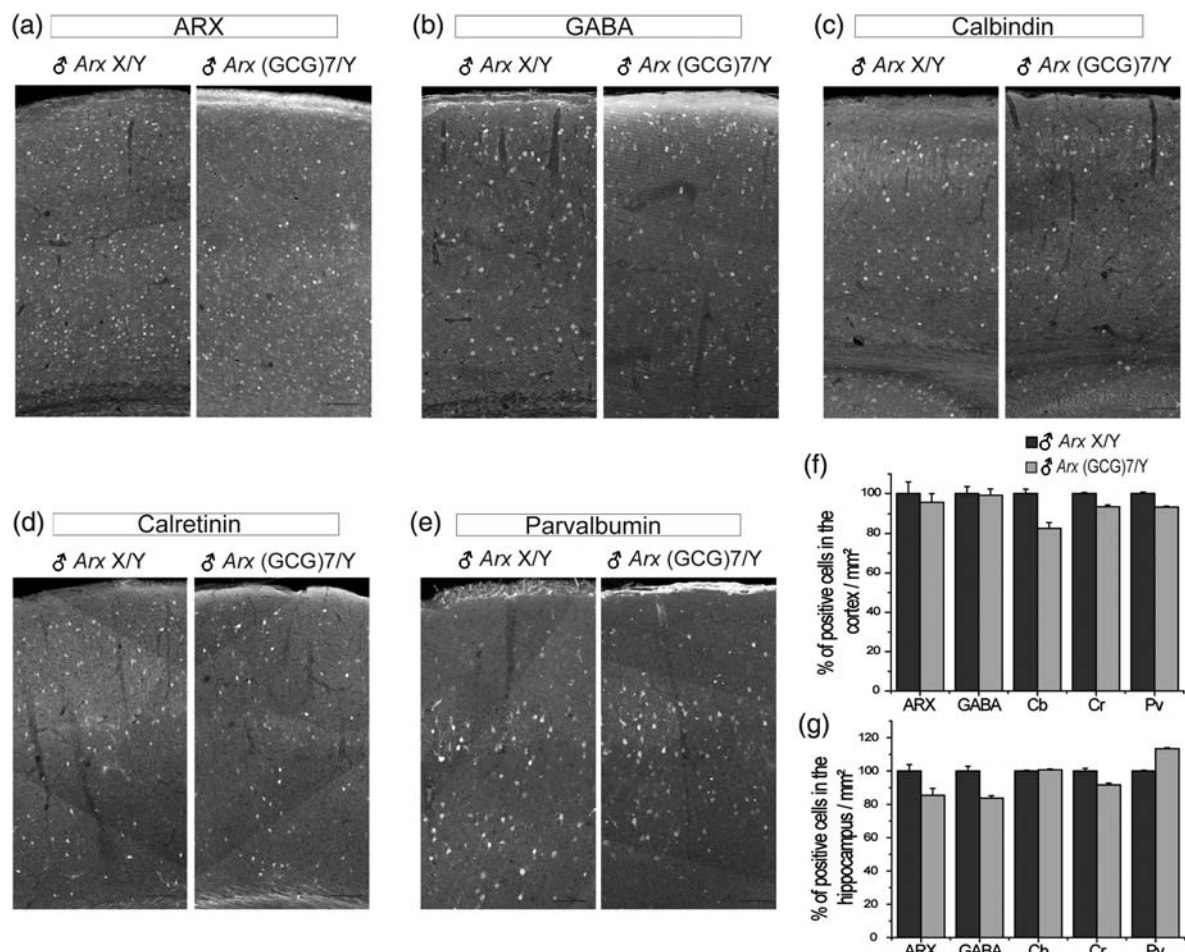


Figure 1. Cortical and hippocampal interneurons are preserved in $Arx^{(GCG)7/Y}$ mice. (a–e) Immunostaining performed on cortical coronal sections at P14–P15 from $Arx^{X/Y}$ mice as control or $Arx^{(GCG)7/Y}$ mice with 1 of the following antibodies: (a) ARX; (b) GABA; (c) Calbindin (Cb); (d) Calretinin (Cr); and (e) Parvalbumin (Pv). Scale bar: 100 μ m. (f) Quantification of immunostaining showing the percentage (\pm SEM) of positive cells in the cortex per mm². No significant changes were found in the $Arx^{(GCG)7/Y}$ compared with the $Arx^{X/Y}$ values considered as 100% for each staining. $Arx^{X/Y}$ $n = 7$ and $Arx^{(GCG)7/Y}$ $n = 12$ for ARX, GABA, and Calretinin antibodies; $Arx^{X/Y}$ $n = 6$ and $Arx^{(GCG)7/Y}$ $n = 6$ for Calbindin and Parvalbumin antibodies. (g) Quantification of immunostaining performed in the hippocampus (Supplementary Fig. S2), showing the percentage of positive cells in the hippocampus per mm². No significant changes were found in the $Arx^{(GCG)7/Y}$ mice compared with the $Arx^{X/Y}$ mice. $Arx^{X/Y}$ $n = 7$ and $Arx^{(GCG)7/Y}$ $n = 12$ for ARX, GABA, and Calretinin antibodies. $Arx^{X/Y}$ $n = 6$ and $Arx^{(GCG)7/Y}$ $n = 6$ for Calbindin and Parvalbumin antibodies.

Migration of Pyramidal Neurons and Cortical Layering are Unaffected by ARX(GCG)7 Mutation

Arx protein is expressed by neural progenitors in the cortical ventricular zone (VZ), but not by radially migrating pyramidal neurons (Colombo et al. 2004; Poirier et al. 2004; Fricourt et al. 2006). Since some defects in the organization of pyramidal neurons have been reported in patients with XLAG (Okazaki et al. 2008) and also in Arx mutant mice (Kitamura et al. 2002), this gene has been proposed to play a role in the migration of cortical pyramidal neurons. In addition, Arx knockdown or its overexpression after in utero electroporation was reported to impair pyramidal cell migration (Fricourt et al. 2008). We thus investigated whether the ARX(GCG)7 mutation alters the migration of cortical pyramidal neurons. To examine this issue, we transfected neural progenitors in the cortical VZ of E14 $Arx^{(GCG)7}$ mouse embryos with RFP expression plasmids in order to visualize migrating pyramidal neurons. Four days later, in both $Arx^{X/Y}$ and $Arx^{X/X}$ mice, RFP-expressing cells had reached the cortical plate (Fig. 3a). We observed the same phenotype in $Arx^{(GCG)7/X}$ heterozygous females (Fig. 3b). Importantly, the migration of

pyramidal neurons was also found to be unaffected in $Arx^{(GCG)7/Y}$ males (Fig. 3c), suggesting that ARX(GCG)7 mutation has no impact on migration of this cell type (Fig. 3d). To further evaluate this issue, we examined the cortical layering in P14–P15 mice with the ARX(GCG)7 mutation using immunostaining with cortical layer markers: CDP for the II–IV layers (Fig. 3f), FoxP2 for the V and VI layers (Fig. 3g), and Bc11b for the V layer (Fig. 3b). We did not observe any significant difference in the thickness of the cortex or the cortical layers in $Arx^{X/Y}$ and $Arx^{(GCG)7/Y}$ mice (Fig. 3e), and no clusters of ectopic pyramidal neurons were found. Moreover, the hippocampal layering was preserved in mutant mice (Fig. 3i).

Taken together, these data show that the ARX(GCG)7 mutation does not affect cortical pyramidal cell migration and layer organization in the neocortex and hippocampus.

Glutamatergic Drive is Increased in the CA1 Field of $Arx^{(GCG)7}$ Mice

The cause of epilepsy in patients or in mice with ARX(GCG)7 mutations is unknown; however, an imbalance in GABAergic

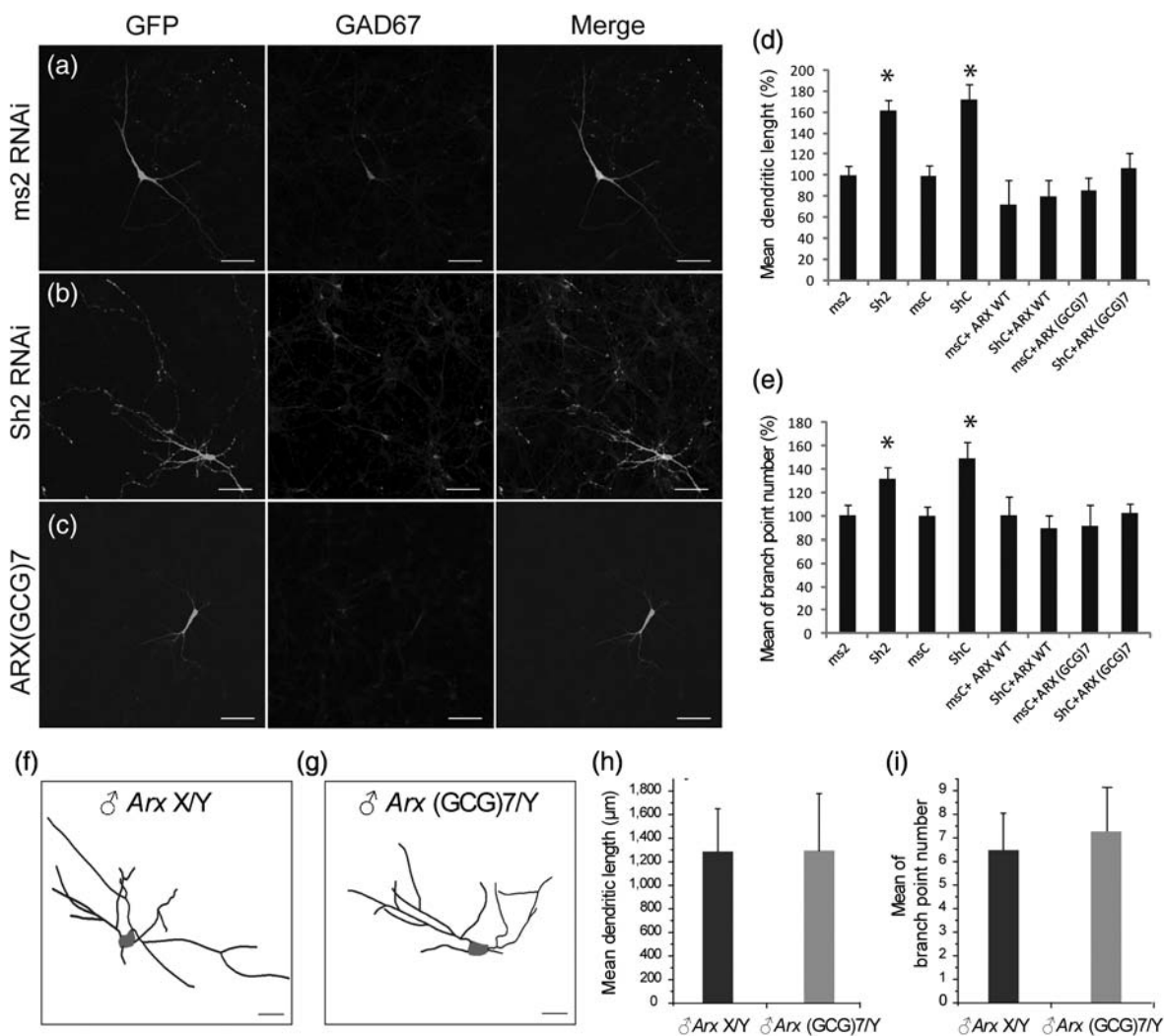


Figure 2. Dendritic arborization of interneurons *in vitro* and *in vivo* is unaffected by ARX(GCG)7 mutation. (a–c) GAD67 immunostaining, on primary rat hippocampal cultures transfected at 3 days *in vitro* (DIV), performed 72 h after transfection with either GFP construct alone or combined with mismatch ms2 construct in (a) or Sh2 RNAi in (b) or ARX(GCG)7 human mutation in (c). Morphology of transfected cells appears in the left column (GFP), and interneurons are specifically identified with the GAD67 immunostaining (middle column). Scale bar: 50 μm . (d) Quantification of the total dendritic length in transfected interneurons. ARX inactivation with Sh2 shRNA significantly increases the interneuron dendritic arborization compared with associated mismatch control considered as 100% (Mann–Whitney test, $*P = 0.009$). The ARX(GCG)7 human mutation and ARX WT human have no effect on the interneurons dendritic arborization compared with control GFP considered as 100% [ms2 RNAi $n = 33$, Sh2 RNAi $n = 36$, msC RNAi $n = 39$, shC RNAi $n = 35$, control GFP $n = 88$, msC + ARX WT $n = 21$, shC + ARX WT $n = 31$, msC + ARX(GCG)7 $n = 39$, shC + ARX(GCG)7 $n = 53$]. Error bars: SEM. (e) Quantification of the number of branch points (% of GFP \pm SEM) in transfected interneurons. ARX inactivation with Sh2 or shC RNAi significantly increases the number of interneuron branch points compared with associated mismatch (Mann–Whitney test, $*P \leq 0.001$). Neither human ARX(GCG)7 nor ARX WT human constructs (whether combined with mismatch or Sh constructs) modified the number of interneuron branch points compared with control GFP considered as 100%. (f) Representative morphology of 1 Arx^{XY} mouse hippocampal interneuron (stratum oriens) after biocytin revelation. Scale bar: 20 μm . (g) Representative morphology of 1 $Arx^{(GCG)7/Y}$ mouse hippocampal interneuron (stratum oriens) after biocytin revelation. Scale bar: 20 μm . (h) Quantification of the total dendritic length (\pm SEM) of hippocampal interneurons (stratum oriens) from Arx^{XY} mice ($n = 6$) or from $Arx^{(GCG)7/Y}$ mice ($n = 6$). No significant changes were found (*t*-test, $P = 0.993$). (i) Quantification of dendritic branch point numbers (\pm SEM) of hippocampal interneurons (stratum oriens) performed in Arx^{XY} mice ($n = 6$) or in $Arx^{(GCG)7/Y}$ mice ($n = 6$). No significant change was found in these mice (Mann–Whitney test, $P = 0.585$).

inhibition is suspected. We investigated this issue by analyzing the EPSCs and IPSCs in CA1 pyramidal cells in acute hippocampal slices from $Arx^{(GCG)7/Y}$ and Arx^{XY} mice (P15–P17); the intrinsic properties of the CA1 pyramidal cells were also investigated (Fig. 4*a–b*). EPSCs were recorded at $V_h = -70$ mV corresponding to the reversal potential for GABAergic currents, and IPSCs were recorded at $V_h = 0$ mV corresponding to the reversal potential for glutamatergic currents. Under these conditions, we observed a strong increase in the EPSC frequency (ca. 40%) in $Arx^{(GCG)7/Y}$ mice ($n = 24$), in comparison with Arx^{XY} mice ($n = 16$) (Fig. 4*c,e*). In contrast, the frequency of IPSCs was not significantly different in both groups

of mice (Fig. 4*c,f*). Accordingly, cell-paired analysis of IPSC/EPSC frequency ratios revealed a drastic decrease (ca. 70%) in $Arx^{(GCG)7/Y}$ mice ($n = 24$) when compared with Arx^{XY} mice ($n = 16$) (Fig. 4*g*). In addition, EPSC and IPSC amplitudes were unaffected in the mutant mouse (18.0 ± 0.9 and 38.25 ± 2.8 pA, respectively; $n = 24$), in comparison with controls (20.3 ± 1.7 and 33.5 ± 3.8 pA, respectively; $n = 16$; $P > 0.05$) (Fig. 4*d*).

This enhanced glutamatergic activity in CA1 pyramidal cells was not associated with significant changes in their intrinsic properties. Thus, in Arx^{XY} ($n = 13$) and $Arx^{(GCG)7/Y}$ ($n = 23$) mice, the resting membrane potential was -61.5 ± 1.9 and

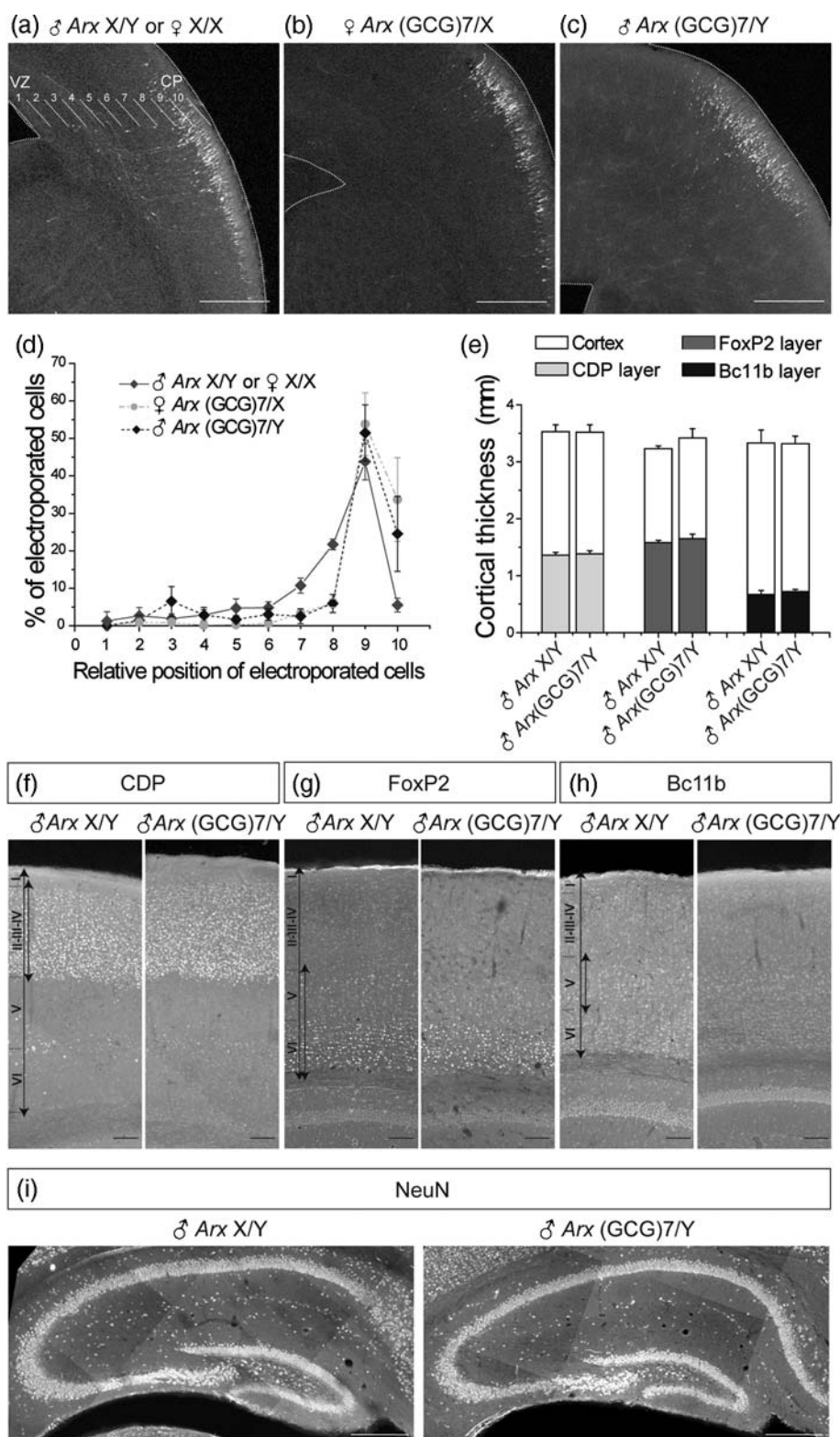


Figure 3. Migration of pyramidal neurons and cortical layering are unaffected by ARX(GCG)7 mutation. (a–c) Coronal sections of mouse brain 4 days after in utero electroporation with RFP control construct to visualize pyramidal cells performed at E14. Electroporated cells in (a) *Arx*^{X/Y} and *Arx*^{X/X} or (b) *Arx*^{(GCG)7/X} mice have reached the cortical plate 4 days after in utero electroporation. (c) *Arx*^{(GCG)7/Y} mice electroporated cells display distribution similar to WT *Arx*^{X/Y}, *Arx*^{X/X}, or *Arx*^{(GCG)7/X} mice. CP, cortical plate. Scale bar: 200 μ m. (d) Quantitative evaluation of the relative position of electroporated cells (\pm SEM) in 10 strata dividing the thickness of the cortex [as seen in (a)] on *Arx*^{X/Y} or *Arx*^{X/X} mice (dark blue, $n = 4$), *Arx*^{(GCG)7/X} mice (light blue, $n = 3$), and *Arx*^{(GCG)7/Y} mice (pink, $n = 3$). No significant differences were detected. (e) Quantification of the cortical size (white) and respective layer size (darkened) identified using specific markers as below (mean mm \pm SEM) on *Arx*^{X/Y} ($n = 7$) or *Arx*^{(GCG)7/Y} ($n = 12$) mice. *Arx*^{(GCG)7/Y} mice have normal cortical layering compared with *Arx*^{X/Y} mice. (f–h) Immunostaining performed at P14–P15 on *Arx*^{X/Y} and *Arx*^{(GCG)7/Y} brains with cortical layer markers: (f) CDP for layers II–IV, (g) FoxP2 for layers V and IV, and (h) Bc11b for layer V. Scale bar: 200 μ m. (i) Immunostaining of hippocampal sections performed at P14–P15 on *Arx*^{X/Y} ($n = 6$) and *Arx*^{(GCG)7/Y} ($n = 6$) mice with the neuronal marker NeuN. Scale bar: 200 μ m.

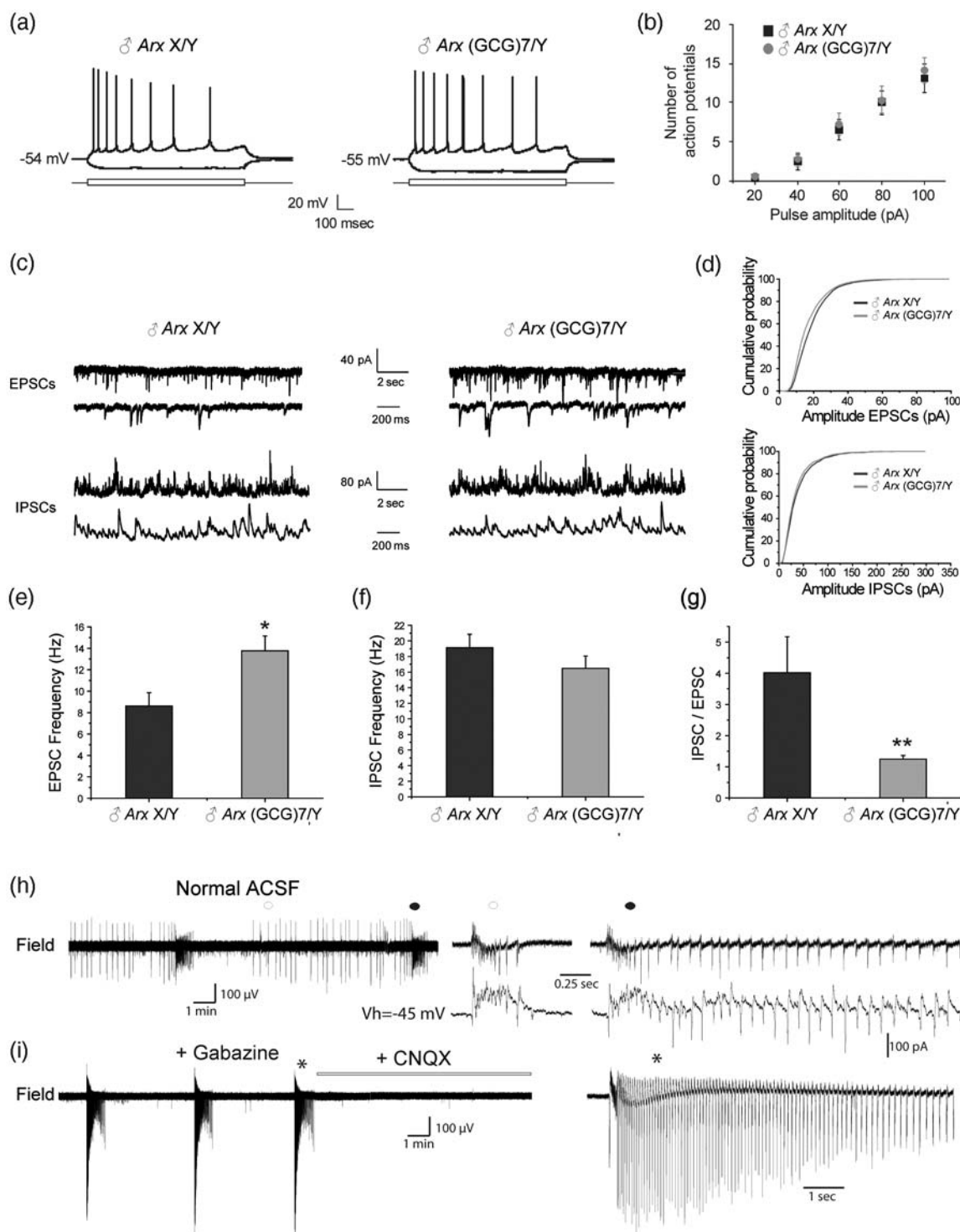


Figure 4. Glutamatergic drive is increased in the CA1 field of $\text{Arx}^{(GCG)7/Y}$ mice. (a) Pattern of discharge of CA1 pyramidal cells from Arx^{XY} (left) and $\text{Arx}^{(GCG)7/Y}$ mice (right) after injection of 60 pA depolarizing and hyperpolarizing current steps (1 s duration) applied from their resting membrane potentials. (b) Average number of action potentials evoked by 20–100 pA current pulses in Arx^{XY} ($n = 12$) and in $\text{Arx}^{(GCG)7/Y}$ mice ($n = 12$). (c) Pattern of spontaneous EPSC ($V_h = -70$ mV) and IPSC ($V_h = 0$ mV) discharge in CA1 pyramidal cells of Arx^{XY} and $\text{Arx}^{(GCG)7/Y}$ mice. (d) Cumulative probability plots for EPSC (top) and IPSC (bottom) amplitude. No significant change was found between Arx^{XY} ($n = 16$) and $\text{Arx}^{(GCG)7/Y}$ mice ($n = 24$, Kolmogorov–Smirnov 2-sample test, $P > 0.05$). (e) Quantification of EPSC frequency on Arx^{XY} ($n = 16$) and $\text{Arx}^{(GCG)7/Y}$ mice ($n = 24$). The mean EPSC frequency (\pm SEM) is significantly increased in $\text{Arx}^{(GCG)7/Y}$ mice (t -test, $*P = 0.013$). (f) Quantification of IPSC frequency on Arx^{XY} ($n = 16$) and $\text{Arx}^{(GCG)7/Y}$ mice ($n = 24$). No significant change was found between Arx^{XY} and $\text{Arx}^{(GCG)7/Y}$ mice ($P > 0.05$). (g) Quantification of cell-paired IPSC/EPSC frequency ratio of Arx^{XY} ($n = 16$) and $\text{Arx}^{(GCG)7/Y}$ mice ($n = 24$). This ratio is significantly decreased in $\text{Arx}^{(GCG)7/Y}$ mice, leading to a significant enhancement of the glutamate drive in these mice (Mann–Whitney test, $**P < 0.001$). (h) Spontaneous interictal and ictal-like epileptiform discharges in CA1 in normal ACSF. Left trace: CA1 field recording. Right trace: interictal and ictal activities at lower time scale at times indicated by symbols on the left trace together with whole-cell patch-clamp recording of a CA1 pyramidal cell in voltage clamp with a KM_2SO_4 field pipette electrode at a membrane potential of -45 mV. At this potential, GABAergic events are outward and glutamatergic events inward. (i) Field recording in the same field than before after addition of gabazine (5 μ M) and subsequent application of 6-cyano-7-nitroquinoxaline-2,3-dione (CNQX) (20 μ M). Note that in the presence of gabazine, the pattern is composed only of ictal-like epileptiform discharges and the large amplification of the signal.

-59.3 ± 1.7 mV; the input resistance was 204 ± 12.5 and 235.1 ± 18.3 M Ω ; and the spike threshold was -33.6 ± 0.97 and -33.2 ± 0.74 mV, respectively. Moreover, the number of action potentials elicited by 5 incremental depolarizing current steps was similar in both groups of mice (Fig. 4*a,b*).

Importantly, we observed in $Arx^{(GCG)7/Y}$ mice a drastic shift in the inhibitory–excitatory synaptic balance toward excitation without any change in the intrinsic membrane properties of CA1 pyramidal neurons. We thus propose that this change in the excitatory drive could promote epileptiform activity. To further assess this hypothesis, we performed field potential recordings in the CA1 area of hippocampal slices from $Arx^{(GCG)7}$ and $Arx^{X/Y}$ mice. In the absence of any pharmacological treatment, we observed spontaneous epileptiform discharges in slices from $Arx^{(GCG)7/Y}$ mice; moreover, we observed both interictal (8 out of 28 slices, average frequency = 0.18 ± 0.06 Hz, and average duration = 1020.8 ± 203.7 ms) and ictal discharges (6 out of 28 slices, average duration = $26\ 231.25$ ms) (Fig. 4*b*).

At single pyramidal cell level, both interictal and ictal activities were characterized by a mixture of GABAergic and glutamatergic events (Fig. 4*b*). Blocking GABA_A receptors with gabazine (5 μ M) changes the recorded pattern, which was then characterized by the presence of ictal-like epileptiform discharges only (Fig. 4*i*). This suggests that in $Arx^{(GCG)7/Y}$ mice, GABA_A receptor activation exerts a strong inhibitory action to prevent the generation of seizures. These activities were fully blocked by 6-cyano-7-nitroquinoxaline-2,3-dione (CNQX) ($n = 3$), suggesting that seizures resulted from an exacerbation of glutamatergic activity. Spontaneous epileptiform activities were never observed in slices from $Arx^{X/Y}$ mice.

We also analyzed the synaptic activity in neocortical slices using whole-cell and field recordings performed in layer II/III. Analysis of field recordings revealed spontaneous interictal-like activities in all slices (7 out of 7 slices, average frequency = 0.08 ± 0.02 Hz, and average duration = 813.7 ± 150 ms) from $Arx^{(GCG)7/Y}$ but not from $Arx^{X/Y}$ mice (Supplementary Fig. S3). These network activities were fully blocked by 10 μ M NBQX, an AMPA receptor antagonist (data not shown). Similar activities were observed in layer V/VI recordings ($n = 3$). Interictal-like activities were associated with large glutamatergic (recorded at $V_h = -70$ mV) and GABAergic (recorded at $V_h = 0$ mV) synaptic drives (Supplementary Fig. S3). Calculation of charge transfer of glutamatergic and GABAergic synaptic currents showed a strong enhancement of glutamatergic (by around 7.7 times) and GABAergic (by around 4.5) drive in $Arx^{(GCG)7/Y}$ compared with $Arx^{X/Y}$; glutamatergic charge transfer was $21\ 506.4 \pm 7334$ pF (per 20 s) and $166\ 483.5073 \pm 34\ 012$ pF (per 20 s) in $Arx^{X/Y}$ ($n = 11$) and $Arx^{(GCG)7/Y}$ ($n = 13$, $P < 0.05$), respectively, and GABAergic charge transfer was $111\ 418.9 \pm 30\ 472$ pF (per 20 s) and $500\ 530 \pm 110\ 797$ pF (per 20 s) in $Arx^{X/Y}$ ($n = 11$) and $Arx^{(GCG)7/Y}$ ($n = 13$, $P < 0.05$). Moreover, there was a significant decrease in the GABAergic/glutamatergic charge transfer ratio in $Arx^{(GCG)7/Y}$ compared with $Arx^{X/Y}$ (Supplementary Fig. S3). This change was not associated with a significant decrease in GABA receptor-mediated IPSCs frequency and amplitude (measured between the bursts); the IPSC frequency was 3.9 ± 0.8 Hz ($n = 11$) and 2.0 ± 0.4 Hz ($n = 13$) in $Arx^{X/Y}$ and $Arx^{(GCG)7/Y}$ mice ($P > 0.05$), and the IPSC amplitude was 25 ± 4.4 pA ($n = 11$) and 16.0 ± 2.3 pA ($n = 13$) in $Arx^{X/Y}$ and $Arx^{(GCG)7/Y}$ mice ($P > 0.05$).

It is important to emphasize the uniqueness of these observations because spontaneous epileptiform activities were rarely observed, in the absence of pharmacological treatment, in slices from animal models of epilepsy and/or resected tissue from epileptic patients (Huberfeld et al. 2011; Liotta et al. 2011). All together, these data indicate that this ARX mutation is associated with hyperexcitability of hippocampal and neocortical networks most likely due to an increase in the excitatory drive rather than an inhibitory failure.

Axonal Fibers in CA1 Pyramidal Cells are Abnormal in $Arx^{(GCG)7}$ Mice

The presence of recurrent epileptiform bursts and increased glutamatergic activity, which we observed in the CA1 hippocampal field, are in favor of synaptic remodeling, similar to those reported previously in temporal lobe epilepsy (Esclapez et al. 1999; Lehmann et al. 2000). To address this question, we analyzed the morphology of CA1 pyramidal cells in $Arx^{(GCG)7/Y}$ and $Arx^{X/Y}$ mice. We found that 45% of cells in $Arx^{(GCG)7}$ mice displayed abnormal axonal recurrent fibers, with collateral branches crossing the pyramidal cell layer and terminating into the stratum radiatum (Fig. 5*a,b* and Supplementary Fig. S4). This type of axonal collateral was never observed in $Arx^{X/Y}$ mice. Axonal Sholl analysis revealed that branching in proximal axonal projections (50 μ m from soma) was significantly increased in cells from $Arx^{(GCG)7/Y}$ mice when compared with those from $Arx^{X/Y}$ mice (Fig. 5*c*). Moreover, branching in basal dendrites located 200 μ m away from the soma was significantly increased in cells with recurrent fibers in $Arx^{(GCG)7}$ mice when compared with cells in $Arx^{X/Y}$ mice (Fig. 5*d*). Taken together, these results show that axonal arborization in CA1 pyramidal cells is abnormal in $Arx^{(GCG)7/Y}$ mice and may reflect network reorganization contributing to epilepsy.

Reconstruction analysis of layer II/III cortical neurons from $Arx^{X/Y}$ ($n = 6$) and $Arx^{(GCG)7/Y}$ ($n = 5$) mice did not reveal statistically significant differences in branching and length of dendritic and axonal arborization. However, collateral axons in 2 out of 5 $Arx^{(GCG)7/Y}$ neurons displayed atypical features with an apparent increase in the number of terminals within layer IV and recurrent collateral branches to layers I and II (Supplementary Fig. S3) and features never observed in $Arx^{X/Y}$ neurons.

Discussion

Arx gene is required for the proper migration of cortical and hippocampal GABA interneurons (Kitamura et al. 2002; Colombo et al. 2007; Friocourt et al. 2008). It was thus proposed that the early onset epileptic encephalopathies associated with ARX mutations could be considered as interneuronopathies (Kato and Dobyns 2005). Analyses of reported cases (Shoubridge et al. 2010) indicate that ARX-related syndrome can be segregated at the molecular level into 2 categories: (1) mutations predicted to lead to ARX loss of function associating severe brain malformations (e.g. XLAG syndrome) and (2) polyalanine expansions leading to milder phenotypes with no apparent brain malformation. In this report, we demonstrate that the expansion of the first polyalanine tract of the ARX gene, the most frequent mutation leading to X-linked West syndrome (Stromme et al. 2002) and Ohtahara syndrome (Absoud et al. 2010), does not necessarily

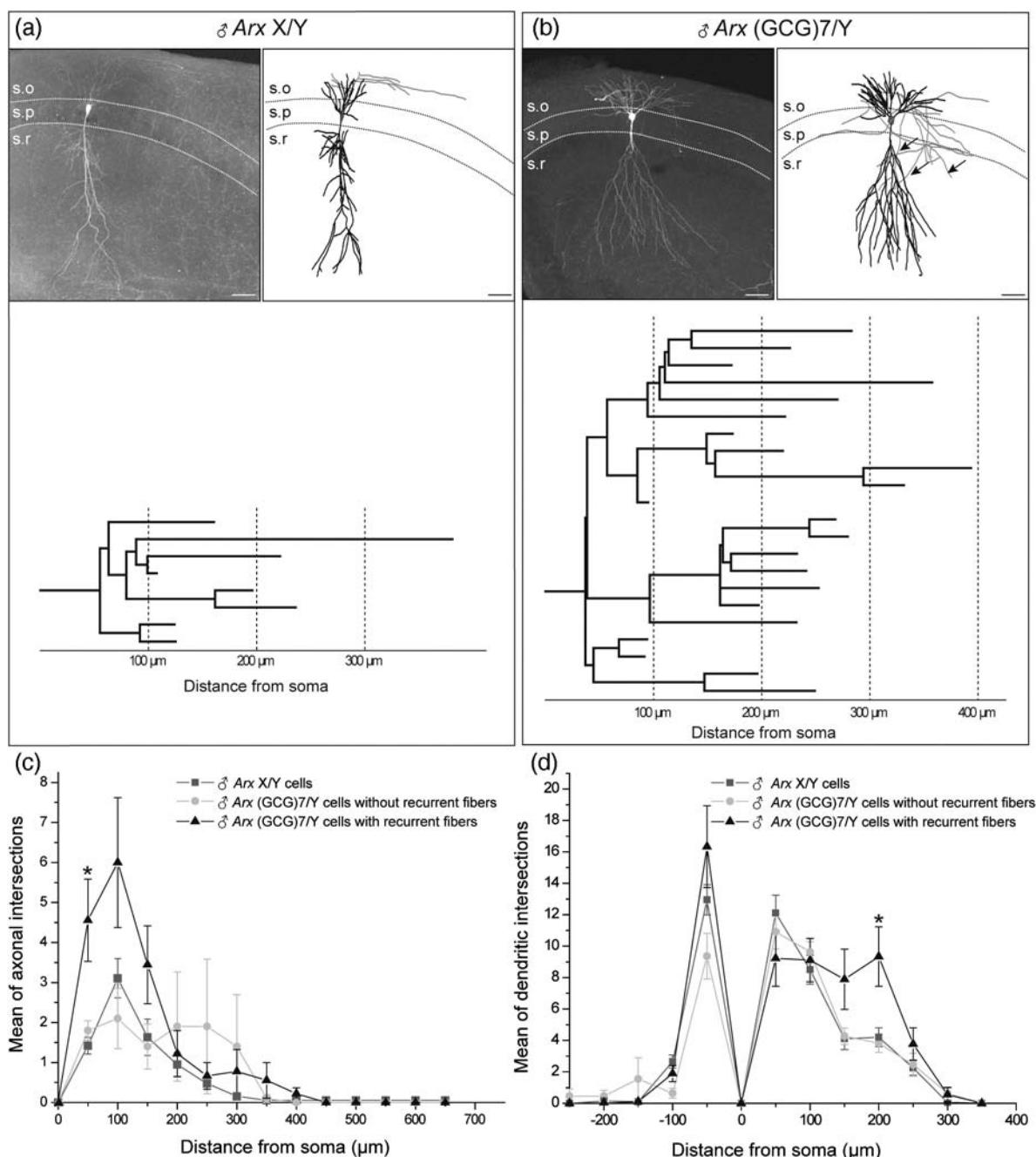


Figure 5. Axonal fibers in CA1 pyramidal cells are abnormal in $Arx^{(GCG)7}$ mice. (a) Confocal image of $Arx^{X/Y}$ mouse CA1 pyramidal cells after biocytin staining (left panel) and its associated NeuroLucida reconstruction (right panel: cell body in green, dendrites in blue, and axon in red). S.o., stratum oriens; S.p., stratum pyramidale; S.r., stratum radiatum. Scale bar: 50 μm . Lower panel shows the axonogram of this cell. (b) Confocal image of $Arx^{(GCG)7/Y}$ mouse CA1 pyramidal cells after biocytin staining (left panel) and its associated NeuroLucida graph reconstruction (right panel: cell body in green, dendrites in blue, and axon in red). CA1 pyramidal cells from $Arx^{(GCG)7/Y}$ mice present abnormal axonal recurrent, reaching the stratum radiatum (arrows). Scale bar: 50 μm . Lower panel shows the axonogram of this cell. (c) Sholl analysis of axons of CA1 pyramidal cells of $Arx^{X/Y}$ mice ($n = 19$, in blue) and $Arx^{(GCG)7/Y}$ mice with recurrent fibers ($n = 9$, in pink) and without recurrent fibers ($n = 10$, in green). The mean number (\pm SEM) of axonal crossings is significantly increased at a distance of 50 μm from the soma when $Arx^{(GCG)7/Y}$ mouse cells present recurrent fibers, compared with cells from $Arx^{X/Y}$ mice (Mann–Whitney test, $*P = 0.004$). (d) Sholl analysis performed on dendrites of CA1 pyramidal cells of $Arx^{X/Y}$ mice ($n = 20$, in blue) and $Arx^{(GCG)7/Y}$ mice cells without recurrent fibers ($n = 11$, in green) or with recurrent fibers ($n = 9$, in pink). Distance from soma -250 to $0 \mu m$ represents apical dendrites, and distance from soma 0 to $350 \mu m$ represents basal dendrites. The mean number (\pm SEM) of basal dendrite crossings is significantly increased at a distance of 200 μm from the soma when $Arx^{(GCG)7/Y}$ mouse cells present recurrent fibers when compared with $Arx^{X/Y}$ mouse cells (Mann–Whitney test, $*P = 0.007$).

alter GABA interneuron development. This notion is supported by 3 different sets of data: (1) the density and distribution of cortical and hippocampal interneurons are normal in mice with ARX(GCG)7 mutation; (2) the dendritic arborization is normal both in cultivated hippocampal interneurons

expressing ARX(GCG)7 human mutation and in brain sections from $Arx^{(GCG)7}$ mice; and (3) the frequency of spontaneous IPSCs in pyramidal neurons from $Arx^{(GCG)7}$ mice is not different from that of controls. Therefore, we propose that ARX mutations can yield either a severe brain malformation

(lissencephaly) related to GABA neuron migration defect associating severe epilepsy, or milder cortical phenotypes with no malformation and no GABA defect but also associating severe epilepsy.

Hence, the data reported here contribute to the clarification of genotype–phenotype correlations in ARX syndrome. Our conclusion, however, is complicated by the complexity and morphofunctional diversity of cortical GABA neuron populations (Klausberger and Somogyi 2008; Gelman and Marín 2010), which could potentially prevent the detection of subtle changes caused by the ARX(GCG)7 mutation. In addition, the phenotype could be altered depending on the genetic background of the mice (Frankel 2009). It was reported in a mixed strain N2 mice (Price et al. 2009) that a similar polyalanine expansion had a moderate impact on cortical interneurons characterized by a selective reduction in Calbindin interneurons without affecting other subtypes. It is also plausible that this mutation delays somehow the migration of GABA neurons (Nasrallah et al. 2011), but these neurons finally succeed to reach the cortical mantle so that inhibition is apparently normal in postnatal mice. Although it has been suggested that alterations in the *Arx* gene can lead to defects in pyramidal cell migration (Fricourt et al. 2008), here we show that the ARX(GCG)7 mutation does not impair radial migration in knock-in mice. Moreover, cortical layering is normal in mice with ARX(GCG)7 mutation, which is consistent with the absence of brain malformation in patients harboring a similar mutation (Guerrini et al. 2007).

The most interesting observation concerns the axonal rearrangement of CA1 pyramidal neurons in *Arx*^{(GCG)7/Y} mice, which apparently form local excitatory recurrent networks. If these exuberant collaterals form functional synaptic contacts, they should contribute to neuronal excitability (the increased frequency of spontaneous EPSCs) and facilitate local synchronization (epileptiform bursts). Moreover, changes on neurotransmitter release probability and/or glutamate receptor expression would contribute concomitantly to epileptogenesis in these mice. Further analyses are required to investigate this issue. It will also be important to evaluate intrinsic and network properties and collateral axon distribution of neocortical neurons from different layers for a better comprehension of cortical alterations observed in mutant mice.

We think that this increased branching and abnormal outgrowth of glutamatergic neuron tree could result from a noncell autonomous mechanism since migrating and differentiating pyramidal neurons do not express *Arx*. However, it can be argued that the transient expression of ARX in neural progenitors is important to a further normal electrophysiological and morphological development. It is important to note, however, that the transfection of GAD67-negative neurons in vitro (putative pyramidal cells) with ARX WT or ARX(GCG)7 constructs does not affect their neuritic outgrowth. It is therefore more reasonable to suggest that pyramidal neurons display in *Arx*^{(GCG)7/Y} mice a noncell autonomous remodeling. The underlying mechanism responsible for this change is not elucidated, but given the pleiotropic actions of GABA in developmental brain (Represa and Ben-Ari 2005), including the modulation of neuritic outgrowth, it is reasonable to suggest that ARX expansion in GABA interneurons would alter its “trophic” actions on surrounding cells.

It is interesting to note that a similar remodeling of axonal networks has been described earlier in the hippocampus of

adult epileptic rats (Esclapez et al. 1999; Lehmann et al. 2000) and was proposed to contribute to epilepsy. In *Arx*^{(GCG)7/Y} mice, this feature would be developmentally acquired and result from either an abnormal axonal outgrowth or a lack of regression of abnormal collaterals observed in immature CA1 pyramidal neurons (Aniksztejn et al. 2001). How the ARX mutation in interneurons actually contributes to this change remains to be elucidated.

It has been well illustrated by Kitamura et al. (2009) that a large majority of *Arx*^{(GCG)7/Y} mice display severe spontaneous seizures starting with limb clonus and progressing to severe tonic-clonic generalized convulsions at the age of 1 month. Here, we show that at P15–P17, some acute hippocampal slices from *Arx*^{(GCG)7/Y} mice display spontaneous seizure-like episodes in the absence of any treatment, whereas slices from most animal models of epilepsy rarely display similar features. The spontaneous epileptic manifestations reported here emphasize the degree of epileptogenicity resulting from the ARX (GCG)7 mutation and its consequences on local cortical networks. Epilepsy in *Arx*^{(GCG)7/Y} mice would originate in the hippocampus and have a glutamatergic origin. However, in 3 recorded animals, Kitamura et al. (2009) found that the first spikes were seen simultaneously in the hippocampus, frontal cortex, and striatum. Although the primary focus was not detected, their observations suggest that the striatum and septum, which experience in *Arx*^{(GCG)7/Y} mice a significant reduction in the number of cholinergic neurons (Kitamura et al. 2009), could also play a major role in seizure expression. To conclude, we propose that epilepsy in *Arx*^{(GCG)7/Y} mice could appear as a consequence of a developmental alteration secondary to the initial gene mutation. We recently reported in a rat model of subcortical band heterotopia that alterations are observed not only in the malformation itself, but also in the normal cortex surrounding the malformation, where an increased glutamatergic drive but no GABAergic alterations was found (Ackman et al. 2009). Therefore, neuronal network remodeling during abnormal cortical development could be a common feature underlying epilepsy in such developmental disorders. Synaptic remodeling could modify the initial phenotype, contribute to the diversity of clinical manifestations linked to single gene mutations, and account for the protracted delay between the initial lesion and the onset of clinical epilepsy.

Supplementary Material

Supplementary material can be found at: <http://www.cercor.oxfordjournals.org/>.

Funding

This study was funded by Agence Nationale de la Recherche (RPV06055ASA), European Community contract no. LSH-CT-2006-037315 (EPICURE) FP6—Thematic priority LIFESCIHEALTH, Fondation pour la recherche médicale 2010, Fondation pour la recherche sur le cerveau—Rotary club de France 2010, INSERM, and Centre National de la Recherche Scientifique to A.R. Toscana Life Sciences Foundation Orphan 01 project to M.P.

Notes

We thank Isabel Jorquera, Emmanuelle Buhler, and Séverine Corby-Pellegrino for technical support; Drs Jean-Bernard Manent and Louisa

Christie for critically reading the manuscript; Dr K. Kitamura and Riken BRC and Mitsubishi Chemical Corporation for kindly providing Arx(GCG)7-1 KI mice; and Drs J. Chelly and P. Collombat for ARX antibodies. *Conflict of Interest:* None declared.

References

- Aboud M, Parr JR, Halliday D, Pretorius P, Zaiwalla Z, Jayawant S. 2010. A novel ARX phenotype: rapid neurodegeneration with Ohtahara syndrome and a dyskinetic movement disorder. *Dev Med Child Neurol.* 52:305–307.
- Ackman JB, Aniksztejn L, Crépel V, Becq H, Pellegrino C, Cardoso C, Ben-Ari Y, Represa A. 2009. Abnormal network activity in a targeted genetic model of human double cortex. *J Neurosci.* 29:313–327.
- Aniksztejn L, Demarque M, Morozov Y, Ben-Ari Y, Represa A. 2001. Recurrent CA1 collateral axons in developing rat hippocampus. *Brain Res.* 913:195–200.
- Bienvenu T, Poirier K, Friocourt G, Bahi N, Beaumont D, Fauchereau F, Ben Jeema L, Zemni R, Vinet MC, Francis F *et al.* 2002. ARX, a novel Prd-class-homeobox gene highly expressed in the telencephalon, is mutated in X-linked mental retardation. *Hum Mol Genet.* 11:981–991.
- Colombo E, Collombat P, Colasante G, Bianchi M, Long J, Mansouri A, Rubenstein JL, Broccoli V. 2007. Inactivation of Arx, the murine ortholog of the X-linked lissencephaly with ambiguous genitalia gene, leads to severe disorganization of the ventral telencephalon with impaired neuronal migration and differentiation. *J Neurosci.* 27:4786–4798.
- Colombo E, Galli R, Cossu G, Geetz J, Broccoli V. 2004. Mouse orthologue of ARX, a gene mutated in several X-linked forms of mental retardation and epilepsy, is a marker of adult neural stem cells and forebrain GABAergic neurons. *Dev Dyn.* 231:631–639.
- Escalpez M, Hirsch JC, Ben-Ari Y, Bernard C. 1999. Newly formed excitatory pathways provide a substrate for hyperexcitability in experimental temporal lobe epilepsy. *J Comp Neurol.* 408:449–460.
- Frankel WN. 2009. Genetics of complex neurological disease: challenges and opportunities for modeling epilepsy in mice and rats. *Trends Genet.* 25:361–367.
- Friocourt G, Kanatani S, Tabata H, Yozu M, Takahashi T, Antypa M, Raguénès O, Chelly J, Férec C, Nakajima K *et al.* 2008. Cell-autonomous roles of ARX in cell proliferation and neuronal migration during corticogenesis. *J Neurosci.* 28:5794–5805.
- Friocourt G, Poirier K, Rakic S, Parnavelas JG, Chelly J. 2006. The role of ARX in cortical development. *Eur J Neurosci.* 23:869–876.
- Geetz J, Cloosterman D, Partington M. 2006. ARX: a gene for all seasons. *Curr Opin Genet Dev.* 16:308–316.
- Gelman DM, Marín O. 2010. Generation of interneuron diversity in the mouse cerebral cortex. *Eur J Neurosci.* 31:2136–2141.
- Guerrini R, Moro F, Kato M, Barkovich AJ, Shiihara T, McShane MA, Hurst J, Loi M, Tohyama J, Norci V *et al.* 2007. Expansion of the first polyA tract of ARX causes infantile spasms and status dystonicus. *Neurology.* 69:427–433.
- Huberfeld G, Menendez de la Prida L, Pallud J, Cohen I, Le Van Quyen M, Adam C, Clemenceau S, Baulac M, Miles R. 2011. Glutamatergic pre-ictal discharges emerge at the transition to seizure in human epilepsy. *Nat Neurosci.* 14:627–634.
- Kato M, Das S, Petras K, Kitamura K, Morohashi K, Abuelo DN, Barr M, Bonneau D, Brady AF, Carpenter NJ. 2004. Mutations of ARX are associated with striking pleiotropy and consistent genotype–phenotype correlation. *Hum Mutat.* 23:147–159.
- Kato M, Dobyns WB. 2005. X-linked lissencephaly with abnormal genitalia as a tangential migration disorder causing intractable epilepsy: proposal for a new term, “interneuronopathy.” *J Child Neurol.* 20:392–397.
- Kitamura K, Itou Y, Yanazawa M, Ohsawa M, Suzuki-Migishima R, Umeki Y, Hohjoh H, Yanagawa Y, Shinba T, Itoh M *et al.* 2009. Three human ARX mutations cause the lissencephaly-like and mental retardation with epilepsy-like pleiotropic phenotypes in mice. *Hum Mol Genet.* 18:3708–3724.
- Kitamura K, Yanazawa M, Sugiyama N, Miura H, Iizuka-Kogo A, Kusaka M, Omichi K, Suzuki R, Kato-Fukui Y, Kamiirisa K. 2002. Mutation of ARX causes abnormal development of forebrain and testes in mice and X-linked lissencephaly with abnormal genitalia in humans. *Nat Genet.* 32:359–369.
- Klausberger T, Somogyi P. 2008. Neuronal diversity and temporal dynamics: the unity of hippocampal circuit operations. *Science.* 321:53–57.
- Korff CM, Nordli DRJ. 2006. Epilepsy syndromes in infancy. *Pediatr Neurol.* 34:253–263.
- Lehmann TN, Gabriel S, Kovacs R, Eilers A, Kivi A, Schulze K, Lankisch WR, Meencke HJ, Heinemann U. 2000. Alterations of neuronal connectivity in area CA1 of hippocampal slices from temporal lobe epilepsy patients and from pilocarpine-treated epileptic rats. *Epilepsia.* 41(Suppl. 6):S190–S194.
- Liotta A, Caliskan G, ul Haq R, Hollnagel JO, Rösler A, Heinemann U, Behrens CJ. 2011. Partial disinhibition is required for transition of stimulus-induced sharp wave-ripple complexes into recurrent epileptiform discharges in rat hippocampal slices. *J Neurophysiol.* 105:172–187.
- Marcorelles P, Laquerriere A, Adde-Michel C, Marret S, Saugier-Verber P, Beldjord C, Friocourt G. 2010. Evidence for tangential migration disturbances in human lissencephaly resulting from a defect in LIS1, DCX and ARX genes. *Acta Neuropathol.* 120:503–515.
- Nabbout R, Dulac O. 2008. Epileptic syndromes in infancy and childhood. *Curr Opin Neurol.* 21:161–166.
- Nasrallah MP, Cho G, Putt ME, Kitamura K, Golden JA. 2011. Differential effects of a polyalanine tract expansion in Arx on neural development and gene expression. *Hum Mol Genet.* 21:1090–1098.
- Okazaki S, Ohsawa M, Kuki I, Kawawaki H, Koriyama T, Ri S, Ichiba H, Hai E, Inoue T, Nakamura H. 2008. Aristaless-related homeobox gene disruption leads to abnormal distribution of GABAergic interneurons in human neocortex: evidence based on a case of X-linked lissencephaly with abnormal genitalia (XLAG). *Acta Neuropathol.* 116:453–462.
- Poirier K, Van Esch H, Friocourt G, Saillour Y, Bahi N, Backer S, Souil E, Castelneau-Ptakhine L, Beldjord C, Francis F. 2004. Neuroanatomical distribution of ARX in brain and its localisation in GABAergic neurons. *Brain Res Mol Brain Res.* 122:35–46.
- Price MG, Yoo JW, Burgess DL, Deng F, Hrachovy RA, Frost JD Jr, Noebels JL. 2009. A triplet repeat expansion genetic mouse model of infantile spasms syndrome, Arx(GCG)10+7, with interneuronopathy, spasms in infancy, persistent seizures, and adult cognitive and behavioral impairment. *J Neurosci.* 29:8752–8763.
- Represa A, Ben-Ari Y. 2005. Trophic actions of GABA on neuronal development. *Trends Neurosci.* 28:278–283.
- Shoubridge C, Cloosterman D, Parkinson-Lawrence E, Brooks D, Geetz J. 2007. Molecular pathology of expanded polyalanine tract mutations in the Aristaless-related homeobox gene. *Genomics.* 90:59–71.
- Shoubridge C, Fullston T, Geetz J. 2010. ARX spectrum disorders: making inroads into the molecular pathology. *Hum Mutat.* 31:889–900.
- Stromme P, Mangelsdorf ME, Scheffer IE, Geetz J. 2002. Infantile spasms, dystonia, and other X-linked phenotypes caused by mutations in Aristaless related homeobox gene, ARX. *Brain Dev.* 24:266–268.